ACS APPLIED NANO MATERIALS

www.acsanm.org

Article

Influence of Magnetic Nanoparticle Degradation in the Frame of Magnetic Hyperthermia and Photothermal Treatments

Yilian Fernández-Afonso, Laura Asín, Lilianne Beola, Raluca M. Fratila,* and Lucía Gutiérrez*

Cite This: *ACS Appl. Nano Mater.* 2022, 5, 16220−16230

Read Online

ACCESS | Metrics & More | Article Recommendations | Supporting Information

ABSTRACT: This work aims at studying how the transformations that magnetic nanoparticles suffer in vivo affect their heating properties in the frame of hyperthermia treatments. Iron oxide magnetic nanoparticles (≈13 nm) with two different coatings [PMAO (polymaleic anhydride-*alt*-1-octadecene) and DMSA (dimercaptosuccinic acid)] have been subjected to an accelerated degradation in a medium simulating lysosome conditions. The particles physicochemical properties (size, size distribution, and magnetic properties) have been followed over the degradation process along 24 days. It was found that DMSA-coated particles degraded much faster than PMAO-coated ones. In addition, their heating properties under both the exposure to an alternating magnetic field or a near infrared light have been tracked along this degradation processes, assessing how the changes in their physicochemical properties affect their heating capacity. Along the degradation procedure, a stronger decrease of the particles heating properties has been observed in the frame of magnetic hyperthermia measurements, in comparison with the photothermal ones. Finally, the PMAO-coated particles have been selected for a degradation study in vivo after intratumoral administration. Interestingly, although the number of particles decreases with time in the tissue, the size and size distribution of the particles do not change significantly over time. This work is especially relevant in the frame of the design of in vivo hyperthermia treatments using magnetic nanoparticles as it would provide fundamental clues regarding the need of repeated doses or the possible use of a single administration depending on the treatment duration.

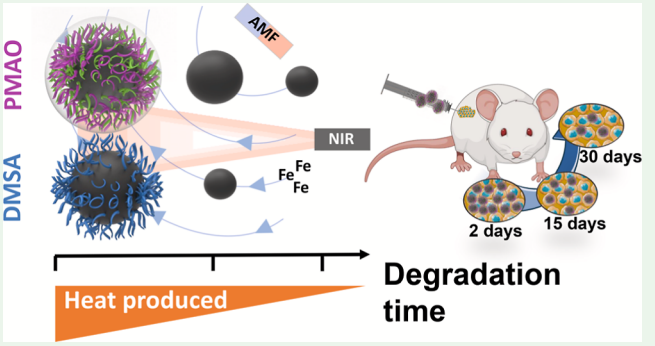

KEYWORDS: *magnetic nanoparticles, iron oxides, degradation, animal models, magnetic hyperthermia, photothermal therapies*

INTRODUCTION

Magnetic nanoparticles (MNPs) and in particular those composed of iron oxides are being used for several in vivo biomedical applications,[1,2] such as drug delivery,[3] imaging,[4] or disease treatments[5] among others. For some of these applications, a single use of the particles is required,[6] meaning that, for example, once the particles have delivered the drug or have been used as contrast agents for imaging purposes, they do not have any further role. Therefore, clearance of the particles from the body afterward would be desirable. In some cases, as for example, in the frame of imaging purposes, particles have been designed to achieve fast renal clearance after their administration.[7] In other cases, it is the iron metabolism of the body the one in charge of the MNP recycling through the particle degradation and iron accumulation in the form of ferritin,[8] a process whose length may vary depending on the particle size, coating, dose, and so forth. However, in some other cases, the particles have a role similar to an implanted medical device for repeated uses (or at least during a given period of time).[9] One of these examples could be the use of MNPs for cancer treatment using magnetic hyperthermia[10] or photothermal therapies.[11] In such an approach, the particles are used as "antennae" able to absorb energy from an external stimulus [either an alternating magnetic field (AMF), a near infrared (NIR) light, or a combination of both] and transform it into local heat. Similar to other classical oncological treatments as chemotherapy or radiotherapy, the magnetic hyperthermia or photothermal therapy approaches are likely to require several cycles in order to achieve a better tumor regression.

In the case of repeated treatments, it is crucial to evaluate the degradation profile of the particles over time. Such studies would provide information about the time frame in which an injected particle remains in a given tissue.[12−15] However, more importantly, in the context of therapy design, it is fundamental to know how any possible particle transformation would affect their performance over time.[16] For instance, in the frame of

Received: July 22, 2022
Accepted: October 14, 2022
Published: October 26, 2022

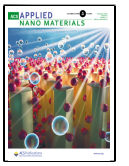

Scheme 1. Scheme of the Iron Oxide Nanoparticle Synthesis and Coating Procedures

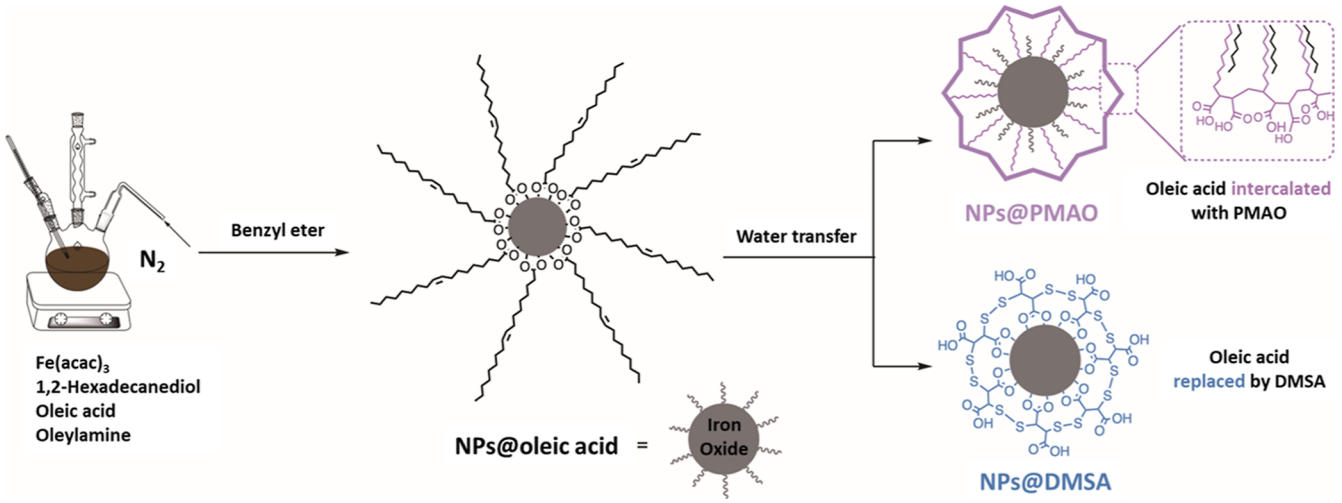

hyperthermia, it has been described that subtle changes in the particle size, shape, or aggregation may have a huge impact on their heating properties.[17,18] Therefore, gathering as much information as possible about the transformations that the particles are undergoing once administered is fundamental to evaluate their suitability for treatment over a long period of time. As a result, in the case of having "viable" particles in the body over a prolonged period of time, a single particle administration could be used, minimizing the discomfort to the patient caused by repeated administrations and lowering the possible risks associated to complicated intratumoral administrations in deep organs. However, in the case of faster degradation processes, repeated nanoparticle administrations would be required to assure the optimal outcome of the treatment.

In this work, we have evaluated how the particle coating affects their degradation profile using a medium that simulates the lysosomal conditions.[19,20] However, we have gone one step forward, tracking how this degradation affects their heating performance in the frame of both magnetic hyperthermia and photothermal treatments. The idea behind this study was to determine how a reduction of the particle size affects their heating performance, which in turn could indicate if a repeated use of the particles would be possible, even if some partial degradation has occurred. From those results, the particles with the longest resistance to degradation were selected and tested in a mouse model in order to evaluate their transformations in vivo over a period of 1 month.

RESULTS AND DISCUSSION

A single batch of MNPs was produced by thermal decomposition, rendering oleic-acid coated nanoparticles that were stored in hexane (Scheme 1). Then, two aliquots of these particles were further treated to produce materials stable in water and coated with two different molecules: poly(maleic anhydride-*alt*-1-octadecene) (PMAO) and dimercaptosuccinic acid (DMSA) (Scheme 1). In both cases (NPs@PMAO and NPs@DMSA), spherical particles with an average core size of ≈13.5 nm were observed by transmission electron microscopy (TEM) after the coating procedure (Figure 1A).

In general, the PMAO-coated particles showed better dispersion in the TEM micrographs than DMSA. Although such observation could be a result of the sample preparation,

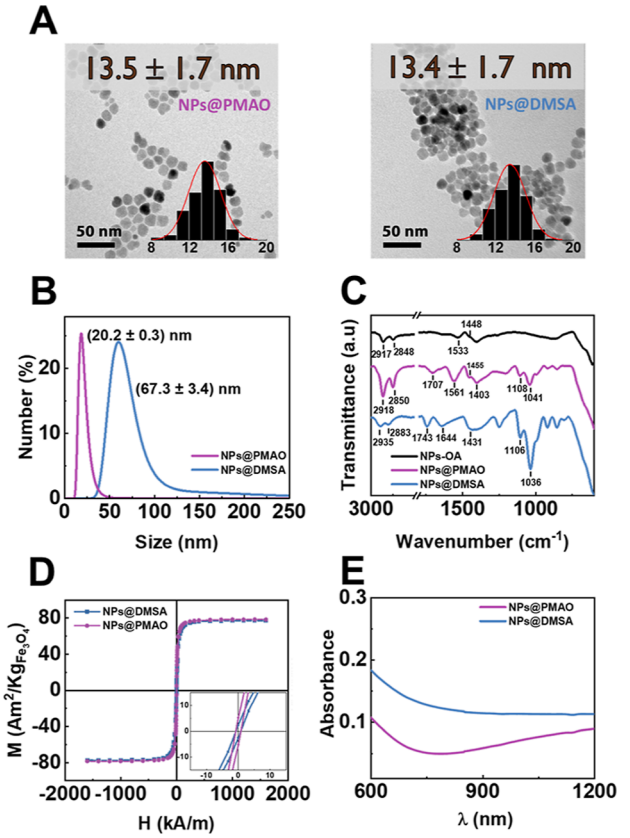

Figure 1. Characterization of MNPs. (A) TEM micrographs and particle size histogram including the size normal distribution function of each type of MNP. (B) Hydrodynamic size distribution obtained by DLS measurements of the MNPs in water. (C) FTIR spectrum of the oleic-acid-coated MNPs and the final nanoparticles after the two different coating procedures. (D) Field-dependent magnetization at room temperature (300 K). (E) UV−vis−NIR spectrum of the nanoparticles with different coatings.

the MNP aggregation after the DMSA coating was also observed by dynamic light scattering (DLS) measurements. In this particular case, NPs@DMSA showed a hydrodynamic diameter of 67.3 ± 3.4 nm, while NPs@PMAO presented a significantly smaller one (20.2 ± 0.3 nm), in agreement with the individual coating of the magnetic cores using this polymer

https://doi.org/10.1021/acsanm.2c03220
ACS Appl. Nano Mater. 2022, 5, 16220−16230

(Figure 1B). In the past, these differences were explained by the crosslinking occurring between several particles during the ligand exchange in the DMSA coating procedure, in contrast with the intercalation of the chains of the polymer (PMAO) with the oleic acid chain that avoided the agglomeration.[21] Therefore, in water, NPs@PMAO behaved as single-core particles, while NPs@DMSA were probably present as multicore particles. The zeta potential (ζ-potential) values of the colloidal suspensions at pH = 7 were −32.7 ± 1.2 and −30.7 ± 2.2 mV for the NPs@PMAO and NPs@DMSA, respectively.

The successful particle coating was also verified by IR observations. In the NPs@PMAO sample, the characteristic C═O bands from PMAO were observed at 1561 and 1707 cm^{-1}.[22] Moreover, C−H bands at 2850 and 2918 cm^{-1} were also identified for that coating. In contrast, the NPs@DMSA sample showed the characteristic C═O stretching bands at 1431 and 1643 cm^{-1}[23] and C−O stretching bands at 1106 cm^{-1} (Figure 1C).[24]

Field-dependent magnetization of the two types of particles showed a superparamagnetic behavior at room temperature (Figure 1D). Although particles had a different coating, as the iron oxide cores from both particles came from the same synthetic batch, the results plotted per mass of magnetite were the same; in both cases, similar remanent magnetization ($M_r \approx 4$ A $m^2/kg_{Fe_3O_4}$), coercive field ($H_c \approx 793$ A/m), and saturation magnetization ($M_s \approx 78$ A $m^2/kg_{Fe_3O_4}$) values were obtained.

Optical absorption was analyzed as this is a fundamental parameter for the characterization of these materials in the frame of photothermal experiments. A decrease in the absorbance from the visible to NIR region was observed for the NPs@DMSA sample (Figure 1E). Additionally, an increase in absorbance was observed for the NPs@PMAO sample in the NIR region. This trend on the wavelength behavior was similar to other reported measurements in the literature.[11]

Tracking of Magnetic Nanoparticle Degradation over Time. One of the objectives of this work was to assess the impact that possible changes in the particles occurring during their degradation in biological media could have on their heating properties under the exposure to both an AMF and an NIR light. For this purpose, it was then fundamental to perform a detailed characterization of the particle's properties along the transformation process.

The degradation procedure was mimicked by placing the two types of particles in a citrate buffer medium (at pH 2.5). Although the lysosomal pH was reported to be 4.5,[25] in the past, stronger acidic media (up to pH = 2.5) were used to speed up the degradation procedure in order to reduce significantly the time needed to observe transformations.[19] In this work, the MNPs ([Fe] = 0.5 mg/mL) were placed in microcentrifuge tubes and maintained at 37 °C in a thermomixer under continuous mixing conditions during 24 days (Figure 2A). Tubes were removed from the thermomixer at selected times to perform the characterization of the colloidal suspensions. Some techniques were only used until shorter times, below 24 days, due to limitations associated to the detection of very small particles or iron ions in the suspensions along the degradation process. The specific time frame in which each technique was used is specified along the text.

An initial characterization of the particles at pH 2.5 was performed (Figure S1). Interestingly, although the hydrodynamic size of NPs@PMAO was very similar in water and in the citrate buffer (20.2 and 24.0 nm, respectively), a bigger change was observed for NPs@DMSA, in which the hydrodynamic size increased from 67.3 to 119.9 nm, indicating the aggregation of the particles in these conditions. Measurements of the ζ-potential values at pH 2.5 indicated a small reduction of the negative charge for NPs@PMAO, from −32.7 to −26.6 mV, and a larger one for the NPs@DMSA ones, from −30.7 to −15.5 mV.

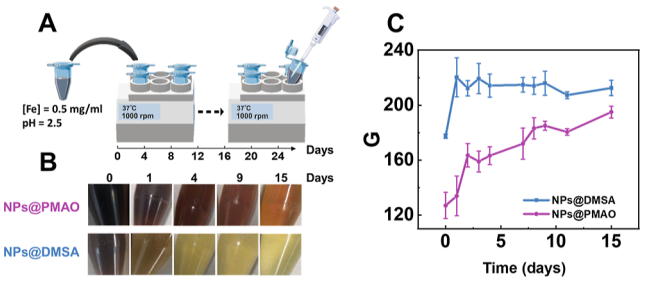

Figure 2. Nanoparticle degradation process. (A) Schematic representation of the degradation experiment. (B) Photos of the nanoparticle suspensions at different times during the degradation process. (C) G parameter values from images acquired at different times during the degradation process.

The degradation procedure was followed by naked eye just through the color change occurring in the colloidal suspension. The liquid color changed from dark brown at the initial time point to yellow in the complete degradation step (Figure 2B; see Figure S2 for the degradation results at pH 4.5). This color transformation was monitored in a more quantitative way through the RGB (red, green, and blue) parameters that describe the suspension color up to day 15.[26] Images of the suspension were acquired with a mobile phone and analyzed with a dedicated app able to determine particle color RGB of the suspension using always the same lightning conditions. This color analysis has been used in the past to monitor changes on iron oxide nanoparticle concentration.[26] In this case, we found that the G parameter was a valid indicator of the particle transformations. In particular, this parameter reached a saturation value of 220 ± 14 two days after the degradation started for NPs@DMSA, while it kept increasing from 127 ± 10 to 195 ± 4 up to day 15 of the experiment for NPs@PMAO (Figure 2C), indicating a still ongoing degradation for the particles with the polymeric coating. The faster degradation of DMSA in comparison with other coatings was previously reported in the literature in in vivo studies.[27]

A drop of the suspension was collected every 24 h and prepared for TEM analysis (Figure 3). Micrographs obtained the first day of the degradation process showed a reduction of the average particle size of NPs@PMAO, resulting in a broader particle size distribution with an average size of 8.6 ± 2.4 nm. In contrast, that same day, the particle size reduction of the NPs@DMSA sample was so large that no particles were observed on the grid. Only a few very small particles could be hardly perceived in the observation conditions. However, given the fact that TEM acquires information at an extremely local level, it was hard to discern if the degradation was complete or a small percentage of particles remained in the sample. A similar behavior was observed for NPs@DMSA at day 15 of the degradation experiment; none of the initial particles were observed. Interestingly, for the sample NPs@PMAO, still a broad distribution of particles sizes was observed at day 15,

https://doi.org/10.1021/acsanm.2c03220
ACS Appl. Nano Mater. 2022, 5, 16220−16230

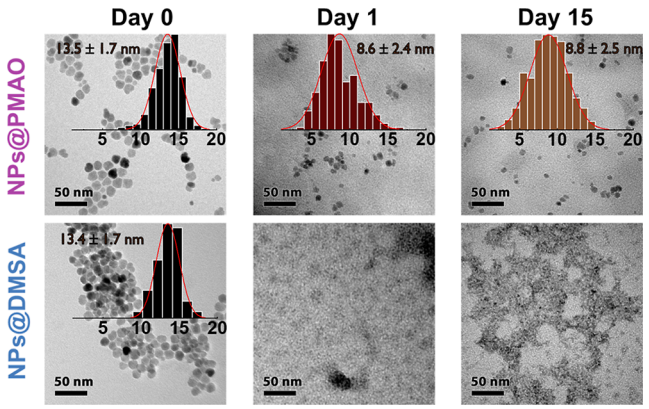

Figure 3. TEM images, histogram, and size normal distribution function of MNPs at different times during the degradation process.

resulting in an average size of 8.8 ± 2.5 nm. It had to be considered that particles with sizes below 1 nm would have been easily neglected in the particle size measurement analysis given the resolution limits of the microscope and the presence of organic matter that complicated the observation of such small sizes.

As mentioned above, TEM is a very local technique that did not allow getting a complete picture of the transformation occurring to the whole sample. Moreover, while TEM analysis at day 15 revealed no presence of particles in the case of the NPs@DMSA sample, suggesting a complete degradation, that was not the case for the NPs@PMAO sample, in which smaller (~9 nm diameter) particles were still detected at that time point. Therefore, to obtain information at longer degradation times and to have a more general picture of the degradation process at the whole sample level, a detailed magnetic characterization was performed. These measurements allowed tracking particle size transformations using a bigger amount of material and thus providing global information about the sample.

Two types of magnetic measurements were performed (AC magnetic susceptibility measurements varying the temperature and field-dependent magnetization curves at 300 K) at different time points along the degradation process of NPs@PMAO and NPs@DMSA (Figure 4).

In the AC magnetic susceptibility measurements, in all cases, the typical maxima in both the in-phase and out-of-phase susceptibility components, which serve as a fingerprint of the presence of MNPs in complex matrices, were observed.[28] The temperature locations of such maxima, being at slightly lower temperatures for the out-of-phase component in comparison with the in-phase one, were indicative of a magnetic relaxation process.[29] Therefore, in order to focus on the temperature locations of the susceptibility maxima along the degradation process, the results were scaled to their maxima (Figure 4A). This type of representation facilitates tracking the changes in temperature locations of the susceptibility maxima informing about the transformations occurring along time.

In the NPs@PMAO sample, a shift in the temperature location of the out-of-phase susceptibility maxima from 170 K at the initial time point to 110 K at 15 days was observed, in agreement with the smaller particle sizes observed by TEM at that time point. Furthermore, transformations continued for longer times, with the out-of-phase susceptibility maximum located at 90 K at 24 days and indicating an ongoing degradation process. In contrast, in the NPs@DMSA sample, a

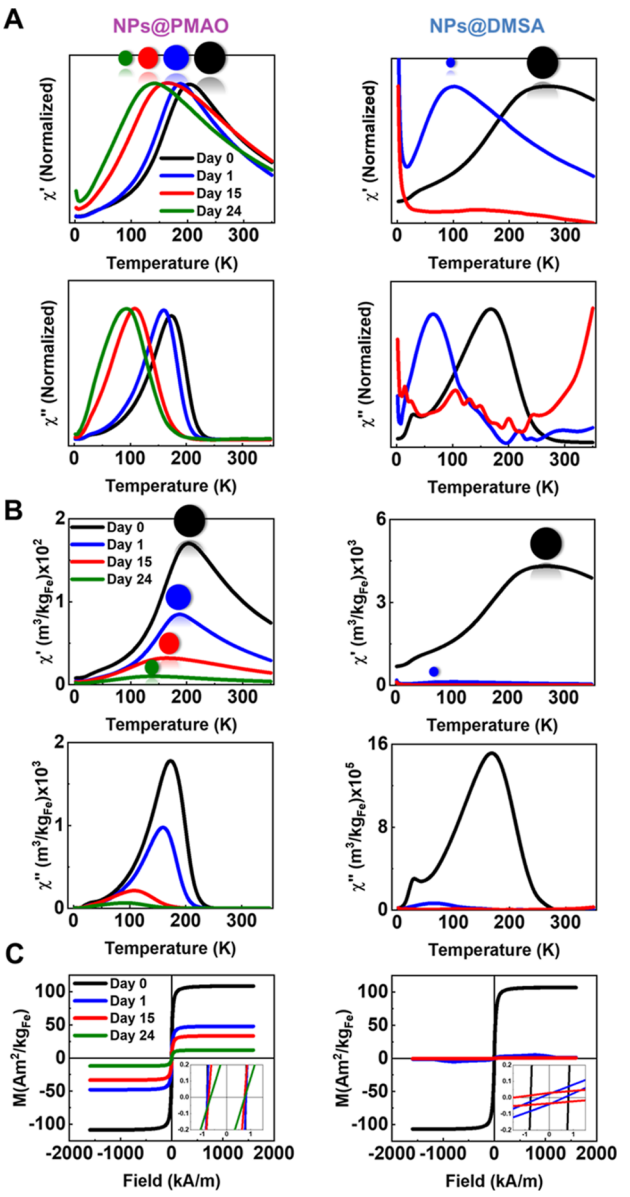

Figure 4. Magnetic characterization of nanoparticle suspensions during the degradation process. (A) In-phase $\chi'(T)$ and out-of-phase $\chi''(T)$ normalized magnetic susceptibility components of the MNPs during the degradation process to observe the differences between the temperatures corresponding to maximum of the signal at different degradation times. (B) In-phase $\chi'(T)$ and out-of-phase $\chi''(T)$ magnetic susceptibility components of the MNPs during the degradation process. (C) Field-dependent magnetization (room temperature) of MNPs at different degradation times.

larger shift (from 170 to 60 K) was already reached 1 day after the degradation process started. At that time point, an additional paramagnetic contribution was observed in the NPs@DMSA sample. The paramagnetic contribution is described by a Curie law behavior that results in a signal that decreases when increasing the temperature,[30] and this is easily observed at the lowest temperatures. This paramagnetic contribution indicated the release of iron atoms from the particle, probably forming a complex with the citrate molecules present in the degradation media. In fact, for the NPs@DMSA sample at the 15 days time point, the main contribution to the magnetic signal was coming from paramagnetic species and not

https://doi.org/10.1021/acsanm.2c03220
ACS Appl. Nano Mater. 2022, 5, 16220−16230

from the initial nanoparticles. In the case of the NPs@PMAO sample, a weak paramagnetic contribution was only observed at the 24 days' time point. This observation did not mean that no iron atoms were released from the particles before that time point; only their magnetic signal per iron atom, much lower than that of the magnetic particles, was under the detection limits of the technique until that time point.

When plotted per mass of sample, the height of the out-of-phase susceptibility maxima acts as a surrogate measurement of the amount of iron in the form of particles in a given sample.[28] In the degradation experiment, a reduction of the out-of-phase susceptibility maxima height along time was observed for both samples. In agreement with the TEM observation, the observed results indicated the decrease of the amount of particles present in the sample as a consequence of the degradation processes. Moreover, the degradation speed identified by the analysis of the out-of-phase susceptibility per mass of iron also revealed a faster degradation for the NPs@DMSA sample when compared to the NPs@PMAO one.

The faster degradation of the NPs@DMSA sample was also clearly visualized in the analysis of the field-dependent magnetization curves, where the saturation magnetization value per mass of iron was ≈107 A m^2/kg_{Fe} at the initial time point for both samples and quickly decreased for the NPs@DMSA sample to 3.7 A m^2/kg_{Fe} just 1 day later, with the reduction of the M_s values along time much slower for the NPs@PMAO sample (48 A m^2/kg_{Fe} at 1 day) (Figure 4C). In this case, the results were plotted per mass of iron, in contrast to the results per mass of magnetite from Figure 1, because the formation of different iron-containing species prevented the use of such units.

From all these results, the RGB color variation, the TEM observations, and the magnetic characterization, it was concluded that the NPs@DMSA sample degraded much faster than the NPs@PMAO one. This behavior was possibly associated to the stronger resistance to degradation of the PMAO coating in the conditions tested, preventing the degradation of the iron core.

Effect of the Degradation on the Particle Heating Properties. It was important to track how the transformations suffered by the particles over the course of their degradation process affected their heating properties, especially considering that in vivo treatments may be repeated several times along long periods of time, using a single particle administration at the beginning of the treatment.[10]

To assess this, the heating produced by the particles when exposed to an external AMF and a NIR light was measured along the degradation process (Figure 5). Both the AC magnetic field and the light power conditions [763.4 kHz and 360 Gauss for the AMF and λ = 1064 nm and power 1.2 W (P/A = 32 W/cm^2) for the NIR light] were above the biosafety limits described for these techniques (5×10^9 A/m s[31] and 1 W/cm^2,[32] respectively). However, these measurement conditions were selected to have a stronger initial heating and therefore be able to track changes in the particle heating capacity within a longer time frame, instead of not being able to track any transformation because of the resolution of our temperature probes.

In both cases (AMF or NIR light exposure), the degradation process resulted in a decrease of the heating capacity of both types of materials. As a result of the faster degradation of the NPs@DMSA particles, the reduction of the heating properties

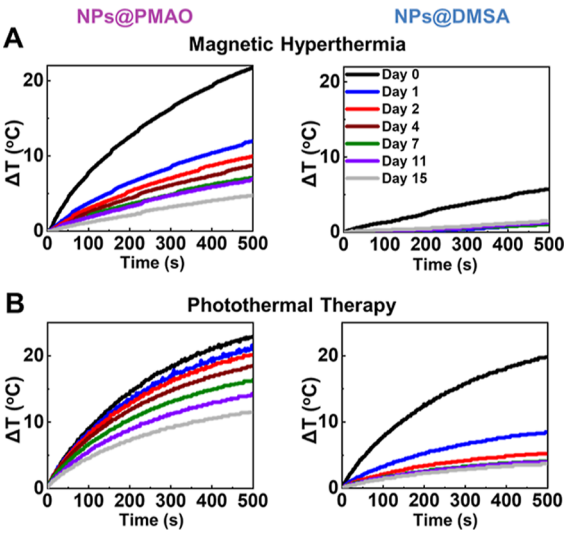

Figure 5. Evaluation of the nanoparticle heating capacity during the degradation process. (A) Magnetic and (B) photothermal characterization of MNPs with different coatings at different times of the degradation process. Suspensions containing always 0.5 mg Fe/mL at different stages of the degradation process were used for both techniques. The AMF used in the magnetic hyperthermia measurements had an amplitude of 360 Gauss and a frequency of 763.4 kHz. The wavelength of the laser light was 1064 nm with a power of 1.2 W (P/A = 32 W/cm^2).

along time was increased for this material when compared to the NPs@PMAO sample.

Interestingly, the heating properties at the initial time point for the NPs@PMAO sample were very similar under the exposure to both an AMF and an NIR light, reaching 22 °C of temperature increase at 500 s time. This coincidence allowed us to easily compare the effect that reductions of the particle size along time had on the heating capacity of the particles in both situations, either AMF or NIR light exposure. The analysis of the NPs@PMAO heating performance indicated that the transformations suffered by the particles had a significantly higher effect in the magnetic hyperthermia experiments when compared to the photothermal ones. One day after the degradation experiment started, the increase in temperature produced by the NPs@PMAO particles was reduced by 45% in the magnetic hyperthermia experiments, while a much smaller reduction, only 4.5%, was measured for the photothermal experiments. Moreover, at day 15 of the degradation experiment, the heating of the particles was reduced by 78% for the magnetic hyperthermia experiments and 48% for the photothermal ones.

In the case of the NPs@DMSA particles, at the initial time point, the heating capacity under NIR exposure was significantly higher than that under the exposure to an AC magnetic field. We assume that this behavior could be due to the aggregation of the DMSA-coated MNPs.[21] Following the same trend observed for the NPs@PMAO ones, the impact of the degradation was much higher on the magnetic hyperthermia experiments in comparison with the photothermal ones.

In the frame of magnetic hyperthermia, it was previously described that small fluctuations on the particle size or particle size distribution have a strong impact on the heating properties of iron oxides,[33] and our results agree with such observations. In contrast, in the frame of photothermal experiments, not so

https://doi.org/10.1021/acsanm.2c03220
ACS Appl. Nano Mater. 2022, 5, 16220−16230

many studies have evaluated the role that particle size has on the heating properties of iron oxides, and in some cases, the obtained results are contradictory and remain under study.[34] If the photothermal heating is related to the band structures of magnetite/maghemite,[35] size should not have a strong impact on the heating, and the changes observed in this work would be attributed to a decrease in the total amount of magnetite/maghemite mass in the sample due to the formation of other iron-containing species, related to the paramagnetic contributions observed in the magnetic characterization data (Figure 4). Our observations indicated a smaller influence of the particle size on the heating properties of particles when exposed to an NIR light than to an AMF, pointing to the fact that the particle degradation along time could have a smaller impact on photothermal therapies in magnetic hyperthermia treatments when performed along long periods of time after particle administration.

In Vivo Tracking of Particle Transformations. The impact of the degradation process was proved to be critical for the particle heating properties. Nevertheless, a simulated degradation in test tubes will never be able to mimic completely the in vivo scenario. Therefore, the NPs@PMAO sample was selected for the in vivo analysis to evaluate the degradation speed of this material in tissue samples. All previous results indicated the faster degradation rate of NPs@DMSA nanoparticles, indicating that the polymeric coating alternative may be more resistant to degradation and therefore more adequate for treatments in which repeated exposures of the animal to the AMF or the NIR light are required.

As discussed before, magnetic susceptibility measurements were selected as an adequate characterization technique, given their capacity to analyze large portions of animal tissues (even complete organs in the case of mice), to track changes in particle size and amount, and to distinguish MNPs from endogenous iron-containing species.[27,28,36] NPs@PMAO particles were intratumorally administered to a xenograft mouse model bearing a pancreatic tumor in one flank. Animals were sacrificed at different time points after the MNP administration and tumor tissues were collected and analyzed magnetically. The analysis of the temperature dependence of the magnetic susceptibility presented the typical behavior of a relaxation process of MNPs already described in the analysis of the degradation in the previous sections.

Interestingly, in contrast with the observations in the simulated lysosomal medium, in this case, minor changes in the temperature-dependence susceptibility profiles were observed in the tumor tissues collected at the three different time points analyzed (2 h and 15 and 30 days after the MNP administration). These "almost" overlapping profiles when scaled to their maximum value (Figure 6A,B) indicated that no major transformations of the particles average size had occurred along 1 month. Indeed, in both cases, a minimal shift of the temperature location of the susceptibility maxima was observed for both coatings. These results are probably linked to a very small increase of the degree of dipolar interactions among the particle magnetic cores, which could be associated to the degradation of the coatings. In the past, some works have reported the biosynthesis of MNPs after degradation processes in stem cells;[37,38] however, given the small differences observed here, this possibility is very unlikely in this case.

Nevertheless, it was also important to analyze the same susceptibility data but plotted per mass of tissue (Figure 6C,D). In such a case, a clear trend of a decrease of the susceptibility maximum height along time was observed in both the in-phase and out-of-phase components. In this type of representation, the height of the susceptibility is a surrogate value of the amount of particles present in the tissues. In fact, it was also possible to quantify the amount of particles in the tumor, assuming that minor transformations had occurred and using as "calibration standard" the signal coming from the administered particles. Using the 150 μg of particles intratumorally injected to the animals as total, only 31% of that dose was found 2 h after the administration. Taking that value as the initial amount of particles in the tumor, then, the percentage of remaining particles from that initial value observed in the tumor decreased until 26% at 30 days after the administration (Figure 6E).

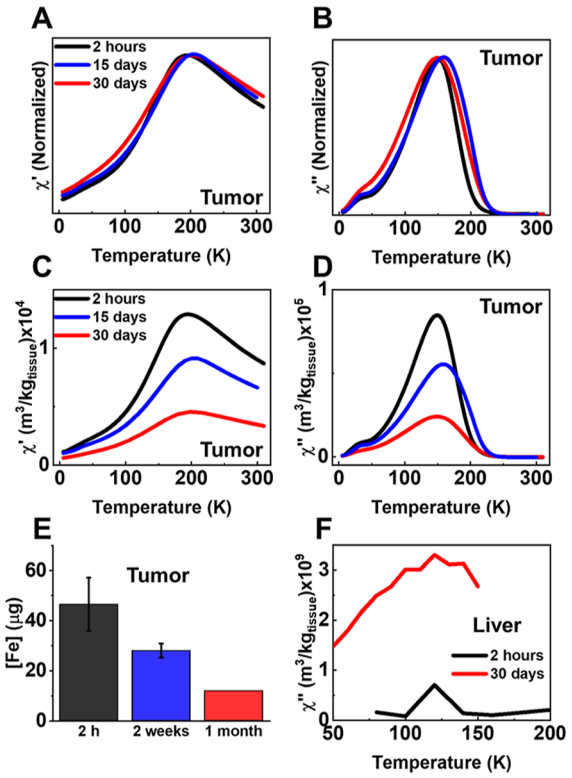

Figure 6. Tissue analysis for the identification and quantification of MNPs (A–E in tumor tissues and F in liver). (A,B) Temperature dependence of the AC magnetic susceptibility profiles of tumor tissues collected at different time points scaled to the maxima value in order to evaluate the particle transformations over time. (C,D) Same results as in panels (A,B) but represented per mass of tissue to evaluate transformations in the amount of particles in the tumors. (E) Iron mass in the form of particles in the tumor tissues collected at different time points, calculated from the out-of-phase susceptibility data represented in (D). (F) Temperature dependence of the AC magnetic susceptibility profile of liver tissues collected at different time points.

Taken together, the results from the magnetic characterization of the tumor samples indicate that although the number of particles decreased along time after their administration, no transformations in the average particle size of particles occurred. In order to explain this, two possible alternatives (or a mixture of both) could have occurred.

One possibility could be that particles could have leaked from the injection site in the tumor tissue to other organs. In fact, intratumoral administration may lead to the location of

https://doi.org/10.1021/acsanm.2c03220
ACS Appl. Nano Mater. 2022, 5, 16220−16230

particles in the periphery of the tumor[39] and in many cases in the extracellular matrix.[40] This inhomogeneous distribution of the particles may be related to their leakage to other organs. In fact, previous works have shown that intratumoral administration of MNPs may lead to their initial accumulation also in the liver and the spleen.[41] However, as far as we know, the continuous transference of particles from the tumor to other organs along time has not been studied in detail yet. Some studies have also described cycles of uptake/release of particles in tumor cell lines.[42] Release of the particles from the cells could have also occurred in our case, transferring the particles to other organs. In fact, in this case, the presence of magnetic particles was detected in liver tissues 1 month after the particle administration probing that some particles had migrated to that organ (Figure 6F). However, the limited number of animals used in this work does not allow to confirm if the presence of particles was produced by a leak along time of the particles to other organs or was a consequence of a non-homogeneous particle distribution resulting from a small initial leak caused during the intratumoral administration (see the different orders of magnitude of the susceptibility data between livers and tumors).

The second possibility could be a heterogeneous degradation of the particles, meaning that not all the particles were degraded simultaneously but in a sequential manner. This behavior has already been described in the past in cell culture models evaluated during periods of times of days. Mazuel et al., using stem cell spheroids, described an "all-or-nothing" degradation, meaning that nanoparticles were either totally dissolved or wholly intact.[43] Our group also found a similar "all-or-nothing" degradation behavior in vitro.[8] However, a more heterogeneous degradation of the particles has been reported when analyzing animal model tissues over longer periods of time (weeks or months).[44−46]

Indeed, both possibilities could have also been occurring at the same time, and further studies will be necessary to elucidate the exact mechanism that explains the decrease of the number of "intact" particles in tumor tissues along time.

Anyway, the degradation process observed in vivo was significantly different from the degradation that occurred in the medium mimicking lysosomal conditions. This difference had also been observed by previous works using MPI (magnetic particle imaging) to track the degradation of MNPs.[47] Therefore, in order to reduce the number of animal experiments, further work should be performed aiming to generate artificial degradation conditions that simulate more accurately the media responsible for the particle degradation in vivo.

Furthermore, our results were fundamental in relation to a key aspect of the development of future cancer treatment plans: the number of AMF exposures and MNP administrations. A recent review on magnetic hyperthermia preclinical methodology revealed that there was no golden standard regarding the number of AFM exposures.[10] The results obtained with the NPs@PMAO particles pointed to the idea that if a single MNP administration is performed and several applications of the AMF are included in the treatment scheme, a reduction of the treatment efficacy along time may occur, mainly due to the decrease of the number of NPs available in the tissue but not because of their size or aggregation transformations over time. These observations highlight the need for monitoring the MNP "disappearance" speed to be able to adjust the therapeutic dose with "booster" MNP re-administrations at certain time points before the re-exposure to the AMF. This could have a significant repercussion on the patient's treatment, depending on the MNP administration route. Until now, most of the preclinical studies on magnetic hyperthermia for cancer treatment (≈80%) used intratumoral administration.[10] This is the preferred route in animal studies as it allows a significant amount of the particles to be delivered to the tumor area. Furthermore, in most cases, animal models generally used are heterotopic models, where the tumor implantation is generally performed subcutaneously in the animal flank, therefore assuring the easy access for a direct intratumoral administration. Nevertheless, going one step further, the direct intratumoral administration of the particles in human patients may result a more complex task, especially when thinking of internal organs affected. In such a case, a single MNP administration requiring some kind of surgery could be bearable if the benefits of the treatment outweigh the risks. However, the need for repeated intratumoral administrations may be a challenge for the medical practice, increasing the risks associated to the treatment and definitely resulting uncomfortable for the patients.

Therefore, we believe that further preclinical work is needed to estimate the clearance of particle speed over time after intratumoral administration, paying especial attention to the physicochemical properties of the material, especially the coating. Thicker coatings with longer times of intact permanence in the tumor may be the clue for successful future cancer treatments.

CONCLUSIONS

When placed in an acid medium mimicking lysosomal conditions, DMSA-coated MNPs degraded much faster than PMAO-coated ones. The transformations that particles suffered along this degradation process had a big impact on their heating properties when exposed to either an AC magnetic field or an NIR laser light, lowering their heating capacity when the particles degraded. This reduction of heating capacity was significantly higher for the case when the heat was produced by the AC magnetic field in comparison with the NIR laser light, suggesting that the particle degradation could have a stronger impact in magnetic hyperthermia treatments in comparison with photothermal therapies.

When tested in vivo, the particle's evolution over time was found to be different from the experiments in an acid medium mimicking lysosomal conditions. After intratumoral injection of PMAO-coated particles, the number of particles decreased over time along 1 month after the particle's administration; however, their size did not change much. It is foreseen then that the particles coming from a single particle administration would preserve their heating properties at least 1 month after their administration. Nevertheless, given the decrease on the number of particles over time, a repetition of the treatment 1 month after the administration would probably not be as efficient as at the initial time point.

This work helps understanding the dynamics of particle transformations in vivo and their impact on the design of therapeutic strategies using the production of heat by MNPs in the frame of cancer treatments.

MATERIALS AND METHODS

Nanoparticle Synthesis. Iron oxide MNPs were synthetized by a seed-mediated thermal decomposition method using an iron(III)

https://doi.org/10.1021/acsanm.2c03220
ACS Appl. Nano Mater. 2022, 5, 16220−16230

acetylacetonate ($Fe(acac)_3$) precursor in the presence of oleic acid (NPs-OA).[48] To generate a hydrophilic surface, the resulting oleic-acid-coated MNPs were modified using two different strategies, an amphiphilic polymer and a small acid. As a first approach, the nanoparticles were coated with an amphiphilic polymer (polymaleic anhydride-*alt*-1-octadecene (PMAO, MW 30,000−50,000 Da)) (NPs@PMAO). Using this protocol, the long hydrophobic aliphatic chains of the polymer intercalate with the oleic acid chain than covers the nanoparticles. As a second approach, 2,3-dimercaptosuccinic acid (DMSA) was used as an iron oxide nanoparticle coating. A procedure of ligand exchange previously described in the past was required to achieve this.[49] The DMSA molecule was coordinated to the surface of the particle replacing the oleic acid coating (NPs@DMSA).

Degradation Process. The nanoparticle degradation with different coatings was evaluated for 24 days. The nanoparticles were dispersed in a citrate buffer solution (from Sigma-Aldrich) at 100 mMol (iron concentration 0.5 mg/mL). This solution was incubated in a thermomixer (Thermomixer Comfort, Eppendorf) at 37 °C using one microtube (1.3 mL) for each time point. In order to accelerate the degradation process, a more acidic pH (pH = 2.5) was used. The incubation was kept under stirring (1000 rpm) to prevent the nanoparticle precipitation during the experiment. Samples were collected along the degradation process at different time points (0, 1, 2, 3, 4, 7, 8, 9, 11, 15, and 24 days) for the subsequent evaluation of the particle transformations with different techniques. Different time points were characterized depending on the technique used for the nanoparticle analysis, and the details are described in the next section.

Nanoparticle Characterization. Before starting the degradation procedure, some basic physicochemical characterization of the particles was performed. The hydrodynamic diameter and zeta potential at pH = 7 and 2.5 of the nanoparticle suspension were measured in a Zetasizer Nano ZS (Malvern). The coating composition was analyzed by Fourier-transformed infrared spectroscopy in an FTIR instrument (FT/IR-4100, JASCO). A nanoparticle suspension (100 μL) at 0.1 mg/mL was placed into a quartz cuvette (3 mm optical path), and absorbance spectrums were acquired on a UV−vis−NIR Spectrophotometer (JASCO V670) in a wavelength interval between 600 and 1200 nm.

Three different techniques were used to track the physicochemical properties of the particles at different time points along their degradation: RGB analysis, TEM, and magnetic measurements. First, the nanoparticle transformation during the degradation was also studied by the suspension color. Images were acquired with a smartphone "Samsung J3" (at 0, 1, 2, 3, 4, 7, 8, 9, 11, and 15 days) using the ColorGrab app (v 3.6.1 Loomatix Ltd.) with controlled lightning conditions. RGB coordinates were analyzed as a function of time.[26] Then, the nanoparticle size and shape were measured at 0, 1, and 15 days of the degradation through TEM observations. Samples were prepared by placing a drop of the diluted suspension onto a carbon-coated grid and allowing it to dry at room temperature. Images were acquired on a Tecnai G2 TEM (FEI) operated at 200 kV. Finally, the influence of the degradation in the particle magnetic properties was studied through AC magnetic susceptibility measurements as a function of temperature and field-dependent magnetization at 300 K. A volume (100 μL) of the solution was collected at different time points along the degradation process (0, 1, 15, and 24 days; 24 days only for NPs@PMAO). The liquid suspension was placed inside a cotton ball, allowing it to dry. Then, this piece of cotton was placed in a gelatin capsule for the magnetic characterization. Magnetic measurements were performed in a Quantum Design MPMS-XL SQUID magnetometer. AC magnetic susceptibility measurements were performed with a field amplitude of 326 A/m and a frequency of 11 Hz, and the field-dependent magnetization was measured at 300 K with a maximum field of 1600 kA/m.

Evaluation of Nanoparticle Transformations on Their Heating Capacity. The nanoparticle heating capacity was studied by magnetic hyperthermia and photothermal conversion measurements during the degradation process. For this, a volume of 1 mL of suspension was collected at different time points of the degradation experiment (0, 1, 2, 3, 4, 7, 8, 9, 11, and 15 days). Magnetic hyperthermia measurements were performed using commercial equipment (D5 Series, nB nanoScale Biomagnetics). The suspension (1 mL) was placed into a glass vial located at the center of the magnetic induction coil inside an isolating holder. The temperature increase over time was recorded at a frequency of 763.4 kHz and a magnetic field amplitude of 360 Gauss using a fiber optic sensor.

The photothermal conversion was evaluated by temperature variation of the solution under the exposure to an NIR light. The same nanoparticle suspension used for the magnetic hyperthermia characterization (1 mL) was placed into a quartz cuvette (1 cm optical path) with magnetic stirring to prevent the nanoparticle precipitation and to homogenize the temperature in the solution. The sample was irradiated during 10 min (Laser Quantum, mpc6000/Ventus 1064 of λ = 1064 nm and beam diameter 2.2 mm) using a power of 1.2 W while recording the suspension temperature with a thermocouple T-type coupled to a Datalogger USB (TC Direct).

In Vivo Experiments and Tumor Tissue Characterization. Six immunodeficient mice, pathogen-free female athymic nude mice (Hsd:Athymic nude-Foxn1nu), 6 weeks old, were purchased from Envigo Laboratory and maintained in the Animal facilities of the Centro de Investigaciones Biomédicas de Aragón (CIBA, IACS-Universidad de Zaragoza). Before any procedure, mice were held 1 week after arriving for acclimation. Animals were maintained according to the institutional animal use and care regulation of the CIBA. All animal experiments were conducted according to the law RD53/2013 and approved by the Ethics Committee for animal experiments from the University of Zaragoza, which is an accredited animal welfare body.

Animals were inoculated with human pancreatic cancer cells (MIA PaCa-2 cells, 5 million). Then, when the tumor grew to sizes ≈0.1 mm^3, 150 μg of iron in the form of NPs@PMAO suspended in PBS was injected intratumorally using a 30 G needle. Mice were then divided randomly into three different groups, one group for each time point for the sacrifice, 2 h and 15 and 30 days after the particle administration. Mice were euthanized by cervical dislocation. Subcutaneous tumors from euthanized mice were removed and freeze-dried in a Telstar cryodos-50 during 24 h. Dried tumors were then placed into gelatin capsules for the magnetic characterization. AC magnetic susceptibility measurements of tumor tissues were performed in the same experimental conditions as described above for the particle suspensions.

■ ASSOCIATED CONTENT

Supporting Information

The Supporting Information is available free of charge at https://pubs.acs.org/doi/10.1021/acsanm.2c03220.

Characterization of the magnetic nanoparticles in the lysozyme-like medium at pH = 2.5 and photos of nanoparticle suspensions at different times during the degradation process (PDF)

■ AUTHOR INFORMATION

Corresponding Authors

Raluca M. Fratila − *Instituto de Nanociencia y Materiales de Aragón (INMA), CSIC-Universidad de Zaragoza, Zaragoza 50018, Spain; Centro de Investigación Biomédica en Red de Bioingeniería, Biomateriales y Nanomedicina (CIBER-BBN), Zaragoza 50018, Spain; Departamento de Química Orgánica, Universidad de Zaragoza, Zaragoza 50009, Spain;* orcid.org/0000-0001-5559-8757; Email: rfratila@unizar.es

Lucía Gutiérrez − *Instituto de Nanociencia y Materiales de Aragón (INMA), CSIC-Universidad de Zaragoza, Zaragoza 50018, Spain; Centro de Investigación Biomédica en Red de Bioingeniería, Biomateriales y Nanomedicina (CIBER-BBN), Zaragoza 50018, Spain; Departamento de Química*

https://doi.org/10.1021/acsanm.2c03220
ACS Appl. Nano Mater. 2022, 5, 16220−16230

Analítica, Universidad de Zaragoza, Zaragoza 50009, Spain; orcid.org/0000-0003-2366-3598; Email: lu@unizar.es

Authors

Yilian Fernández-Afonso − *Instituto de Nanociencia y Materiales de Aragón (INMA), CSIC-Universidad de Zaragoza, Zaragoza 50018, Spain; Departamento de Química Analítica, Universidad de Zaragoza, Zaragoza 50009, Spain;* orcid.org/0000-0002-0970-1917

Laura Asín − *Instituto de Nanociencia y Materiales de Aragón (INMA), CSIC-Universidad de Zaragoza, Zaragoza 50018, Spain; Centro de Investigación Biomédica en Red de Bioingeniería, Biomateriales y Nanomedicina (CIBER-BBN), Zaragoza 50018, Spain;* orcid.org/0000-0003-0641-3407

Lilianne Beola − *Instituto de Nanociencia y Materiales de Aragón (INMA), CSIC-Universidad de Zaragoza, Zaragoza 50018, Spain;* Present Address: Istituto Italiano di Tecnologia, Smart Bio-Interfaces, Viale Rinaldo Piaggio 34, 56025 Pontedera, Italy; orcid.org/0000-0003-4516-8694

Complete contact information is available at: https://pubs.acs.org/10.1021/acsanm.2c03220

Author Contributions

The manuscript was written through contributions of all authors. All authors have given approval to the final version of the manuscript.

Funding

This work was funded by the Ministerio de Ciencia, Innovación y Universidades (MCIU), the Agencia Estatal de Investigación (AEI), and Fondo Europeo de Desarrollo Regional (FEDER) through the MACBETH project (PGC2018-096016-B-I00 to R.M.F. and L.G.). Funding was also received from the European Commission through the TBMED project (DT-NMBP-02-2018, ID: 814439 to R.M.F.). The authors also acknowledge support from Gobierno de Aragón and Fondos FEDER for funding the Bionanosurf (E15_17R) research group. MINECO and FSE/Agencia Estatal de Investigación are also acknowledged for the Ramón y Cajal subprogram grant RYC-2015-17640 to R.M.F. Y.F-A. would like to thank Santander-Universidad Zaragoza Fellowship program for her PhD position.

Notes

The authors declare no competing financial interest.

■ ACKNOWLEDGMENTS

The authors would like to acknowledge the use of Servicios Científicos Técnicos del CIBA (IACS-Universidad de Zaragoza), the Advanced Microscopy Laboratory, for access to their instrumentation and expertise and Servicio General de Apoyo a la Investigación-SAI, Universidad de Zaragoza.

■ REFERENCES

(1) Anik, M. I.; Hossain, M. K.; Hossain, I.; Mahfuz, A. M. U. B.; Rahman, M. T.; Ahmed, I. Recent Progress of Magnetic Nanoparticles in Biomedical Applications: A Review. *Nano Sel.* **2021**, *2*, 1146−1186.

(2) Nabavinia, M.; Beltran-Huarac, J. Recent Progress in Iron Oxide Nanoparticles as Therapeutic Magnetic Agents for Cancer Treatment and Tissue Engineering. *ACS Appl. Bio Mater.* **2020**, *3*, 8172−8187.

(3) Lee, J.-H.; Chen, K.-J.; Noh, S.-H.; Garcia, M. A.; Wang, H.; Lin, W.-Y.; Jeong, H.; Kong, B. J.; Stout, D. B.; Cheon, J.; Tseng, H.-R. On-Demand Drug Release System for In Vivo Cancer Treatment through Self-Assembled Magnetic Nanoparticles. *Angew. Chem., Int. Ed. Engl.* **2013**, *52*, 4384−4388.

(4) Okada, S.; Bartelle, B. B.; Li, N.; Breton-Provencher, V.; Lee, J. J.; Rodriguez, E.; Melican, J.; Sur, M.; Jasanoff, A. Calcium-Dependent Molecular FMRI Using a Magnetic Nanosensor. *Nat. Nanotechnol.* **2018**, *13*, 473−477.

(5) Lu, Y.; Rivera-Rodriguez, A.; Tay, Z. W.; Hensley, D.; Fung, K. L. B.; Colson, C.; Saayujya, C.; Huynh, Q.; Kabuli, L.; Fellows, B.; Chandrasekharan, P.; Rinaldi, C.; Conolly, S. Combining Magnetic Particle Imaging and Magnetic Fluid Hyperthermia for Localized and Image-Guided Treatment. *Int. J. Hyperther.* **2020**, *37*, 141−154.

(6) Cheng, H.; Tsao, H.; Chiang, C.; Chen, S. Advances in Magnetic Nanoparticle-Mediated Cancer Immune-Theranostics. *Adv. Healthcare Mater.* **2021**, *10*, 2001451.

(7) Shin, T. H.; Kim, P. K.; Kang, S.; Cheong, J.; Kim, S.; Lim, Y.; Shin, W.; Jung, J. Y.; Lah, J. D.; Choi, B. W.; Cheon, J. High-resolution T1 MRI via renally clearable dextran nanoparticles with an iron oxide shell. *Nat. Biomed. Eng.* **2021**, *5*, 252−263.

(8) Rojas, J. M.; Gavilán, H.; del Dedo, V.; Lorente-Sorolla, E.; Sanz-Ortega, L.; da Silva, G. B.; Costo, R.; Perez-Yagüe, S.; Talelli, M.; Marciello, M.; Morales, M. P.; Barber, D. F.; Gutiérrez, L. Time-Course Assessment of the Aggregation and Metabolization of Magnetic Nanoparticles. *Acta Biomater.* **2017**, *58*, 181−195.

(9) van Landeghem, F. K. H.; Maier-Hauff, K.; Jordan, A.; Hoffmann, K. T.; Gneveckow, U.; Scholz, R.; Thiesen, B.; Brück, W.; von Deimling, A. Post-Mortem Studies in Glioblastoma Patients Treated with Thermotherapy Using Magnetic Nanoparticles. *Biomaterials* **2009**, *30*, 52−57.

(10) Beola, L.; Gutiérrez, L.; Grazú, V.; Asín, L. *A Roadmap to the Standardization of in Vivo Magnetic Hyperthermia*; Elsevier, 2018; pp 317−337.

(11) Espinosa, A.; Di Corato, R.; Kolosnjaj-Tabi, J.; Flaud, P.; Pellegrino, T.; Wilhelm, C. Duality of Iron Oxide Nanoparticles in Cancer Therapy: Amplification of Heating Efficiency by Magnetic Hyperthermia and Photothermal Bimodal Treatment. *ACS Nano* **2016**, *10*, 2436−2446.

(12) Nosrati, H.; Salehiabar, M.; Fridoni, M.; Abdollahifar, M. A.; Kheiri Manjili, H.; Davaran, S.; Danafar, H. New Insight about Biocompatibility and Biodegradability of Iron Oxide Magnetic Nanoparticles: Stereological and In Vivo MRI Monitor. *Sci. Rep.* **2019**, *9*, 1−10.

(13) Estevanato, L. L. C.; Lacava, L. M.; Carvalho, L. C. F.; Azevedo, R. B.; Silva, O.; Pelegrini, F.; Báo, S. N.; Morais, P. C.; Lacava, Z. G. M. Long-Term Biodistribution and Biocompatibility Investigation of Dextran-Coated Magnetite Nanoparticle Using Mice as the Animal Model. *J. Biomed. Nanotechnol.* **2012**, *8*, 301−308.

(14) Zelepukin, I. V.; Yaremenko, A. V.; Ivanov, I. N.; Yuryev, M. V.; Cherkasov, V. R.; Deyev, S. M.; Nikitin, P. I.; Nikitin, M. P. Long-Term Fate of Magnetic Particles in Mice: A Comprehensive Study. *ACS Nano* **2021**, *15*, 11341−11357.

(15) Levy, M.; Luciani, N.; Alloyeau, D.; Elgrabli, D.; Deveaux, V.; Pechoux, C.; Chat, S.; Wang, G.; Vats, N.; Gendron, F.; Factor, C.; Lotersztajn, S.; Luciani, A.; Wilhelm, C.; Gazeau, F. Long Term in Vivo Biotransformation of Iron Oxide Nanoparticles. *Biomaterials* **2011**, *32*, 3988−3999.

(16) Briley-Saebo, K.; Bjørnerud, A.; Grant, D.; Ahlstrom, H.; Berg, T.; Kindberg, G. M. Hepatic Cellular Distribution and Degradation of Iron Oxide Nanoparticles Following Single Intravenous Injection in Rats: Implications for Magnetic Resonance Imaging. *Cell Tissue Res.* **2004**, *316*, 315−323.

(17) Conde-Leboran, I.; Baldomir, D.; Martinez-Boubeta, C.; Chubykalo-Fesenko, O.; del Puerto Morales, M.; Salas, G.; Cabrera, D.; Camarero, J.; Teran, F. J.; Serantes, D. A Single Picture Explains Diversity of Hyperthermia Response of Magnetic Nanoparticles. *J. Phys. Chem. C* **2015**, *119*, 15698−15706.

(18) Gavilán, H.; Simeonidis, K.; Myrovali, E.; Mazarío, E.; Chubykalo-Fesenko, O.; Chantrell, R.; Balcells, L.; Angelakeris, M.; Morales, M. P.; Serantes, D. How Size, Shape and Assembly of

Magnetic Nanoparticles Give Rise to Different Hyperthermia Scenarios. *Nanoscale* **2021**, *13*, 15631−15646.
(19) Gutiérrez, L.; Romero, S.; da Silva, G. B.; Costo, R.; Vargas, M. D.; Ronconi, C. M.; Serna, C. J.; Veintemillas-Verdaguer, S.; del Puerto Morales, M. Degradation of Magnetic Nanoparticles Mimicking Lysosomal Conditions Followed by AC Susceptibility. *Biomed. Tech.* **2015**, *60*, 417−425.
(20) Lévy, M.; Lagarde, F.; Maraloiu, V.-A.; Blanchin, M.-G.; Gendron, F.; Wilhelm, C.; Gazeau, F. Degradability of Superparamagnetic Nanoparticles in a Model of Intracellular Environment: Follow-up of Magnetic, Structural and Chemical Properties. *Nanotechnology* **2010**, *21*, 395103.
(21) Gutiérrez, L.; de la Cueva, L.; Moros, M.; Mazarío, E.; de Bernardo, S.; de la Fuente, J. M.; Morales, M. P.; Salas, G. Aggregation Effects on the Magnetic Properties of Iron Oxide Colloids. *Nanotechnology* **2019**, *30*, 112001.
(22) Li, L.; Ruotolo, A.; Leung, C. W.; Jiang, C. P.; Pong, P. W. T. Characterization and Bio-Binding Ability Study on Size-Controllable Highly Monodisperse Magnetic Nanoparticles. *Microelectron. Eng.* **2015**, *144*, 61−67.
(23) Çitoğlu, S.; Coşkun, Ö. D.; Tung, L. D.; Onur, M. A.; Thanh, N. T. K. DMSA-Coated Cubic Iron Oxide Nanoparticles as Potential Therapeutic Agents. *Nanomedicine* **2021**, *16*, 925−941.
(24) Keattanong, P.; Wasukan, N.; Kuno, M.; Srisung, S. Synthesis, Structural Characterization, Computational Studies and Stability Evaluations of Metal Ions and ZnONPs Complexes with Dimercaptosuccinic Acid. *Heliyon* **2021**, *7*, No. e05962.
(25) Arbab, A. S.; Wilson, L. B.; Ashari, P.; Jordan, E. K.; Lewis, B. K.; Frank, J. A. A Model of Lysosomal Metabolism of Dextran Coated Superparamagnetic Iron Oxide (SPIO) Nanoparticles: Implications for Cellular Magnetic Resonance Imaging. *NMR Biomed.* **2005**, *18*, 383−389.
(26) Fernández-Afonso, Y.; Salas, G.; Fernández-Barahona, I.; Herranz, F.; Grüttner, C.; Martínez de la Fuente, J.; Puerto Morales, M.; Gutiérrez, L.; Fernández-Afonso, Y.; Salas, G.; Fernández-Barahona, I.; Herranz, F.; Grüttner, C.; Martínez de la Fuente, J.; del Puerto Morales, M.; Gutiérrez, L. Smartphone-Based Colorimetric Method to Quantify Iron Concentration and to Determine the Nanoparticle Size from Suspensions of Magnetic Nanoparticles. *Part. Part. Syst. Charact.* **2020**, *37*, 2000032.
(27) Ruiz, A.; Gutiérrez, L.; Cáceres-Vélez, P. R.; Santos, D.; Chaves, S. B.; Fascineli, M. L.; Garcia, M. P.; Azevedo, R. B.; Morales, M. P. P.; Gutiérrez, L.; Cáceres-Vélez, P. R.; Santos, D.; Chaves, S. B. B.; Fascineli, M. L.; Garcia, M. P.; Azevedo, R. B.; Morales, M. P. Biotransformation of Magnetic Nanoparticles as a Function of Coating in a Rat Model. *Nanoscale* **2015**, *7*, 16321−16329.
(28) Fernández-Afonso, Y.; Asín, L.; Beola, L.; Moros, M.; de la Fuente, M. J.; Fratila, R. M.; Grazú, V.; Gutiérrez, L. Iron Speciation in Animal Tissues Using AC Magnetic Susceptibility Measurements: Quantification of Magnetic Nanoparticles, Ferritin, and Other Iron-Containing Species. *ACS Appl. Bio Mater.* **2022**, *5*, 1879.
(29) García-Palacios, J. L. On the Statics and Dynamics of Magnetoanisotropic Nanoparticles. *Adv. Chem. Phys.* **2000**, *112*, 1−210.
(30) Buschow, K. H. J.; Boer, F. R. *Physics of Magnetism and Magnetic Materials*; Springer, 2003; Vol. 7.
(31) Hergt, R.; Dutz, S. Magnetic particle hyperthermia-biophysical limitations of a visionary tumour therapy. *J. Magn. Magn. Mater.* **2007**, *311*, 187−192.
(32) Ziegelberger, G. ICNIRP Guidelines on Limits of Exposure to Laser Radiation of Wavelengths between 180 nm and 1,000 μm. *Health Phys.* **2013**, *105*, 271−295.
(33) Munoz-Menendez, C.; Conde-Leboran, I.; Baldomir, D.; Chubykalo-Fesenko, O.; Serantes, D. The Role of Size Polydispersity in Magnetic Fluid Hyperthermia: Average vs. Local Infra/over-Heating Effects. *Phys. Chem. Chem. Phys.* **2015**, *17*, 27812−27820.
(34) Paściak, A.; Marin, R.; Abiven, L.; Pilch-Wróbel, A.; Misiak, M.; Xu, W.; Prorok, K.; Bezkrovnyi, O.; Marciniak, L.; Chanéac, C.; Gazeau, F.; Bazzi, R.; Roux, S.; Viana, B.; Lehto, V. P.; Jaque, D.; Bednarkiewicz, A. Quantitative Comparison of the Light-to-Heat Conversion Efficiency in Nanomaterials Suitable for Photothermal Therapy. *ACS Appl. Mater. Interfaces* **2022**, *14*, 33555−33566.
(35) Rivero, M.; Hu, J.; Jaque, D.; Cañete, M.; Sánchez-Marcos, J.; Muñoz-Bonilla, A.; Cañete, M.; Sanchez, J.; Muñoz, A. Compositional Tuning of Light-to-Heat Conversion Efficiency and of Optical Properties of Superparamagnetic Iron Oxide Nanoparticles. *J. Phys. Chem. C* **2018**, *122*, 16389−16396.
(36) Gutiérrez, L.; Lázaro, F. J.; Abadía, A. R.; Romero, M. S.; Quintana, C.; Puerto Morales, M.; Patiño, C.; Arranz, R. Bioinorganic Transformations of Liver Iron Deposits Observed by Tissue Magnetic Characterisation in a Rat Model. *J. Inorg. Biochem.* **2006**, *100*, 1790−1799.
(37) Van de Walle, A.; Plan Sangnier, A. P.; Abou-Hassan, A.; Curcio, A.; Hémadi, M.; Menguy, N.; Lalatonne, Y.; Luciani, N.; Wilhelm, C. Biosynthesis of magnetic nanoparticles from nano-degradation products revealed in human stem cells. *Proc. Natl. Acad. Sci. U.S.A.* **2019**, *116*, 4044−4053.
(38) Curcio, A.; Van de Walle, A.; Serrano, A.; Preveral, S.; Péchoux, C.; Pignol, D.; Menguy, N.; Lefevre, C. T.; Espinosa, A.; Wilhelm, C. Transformation Cycle of Magnetosomes in Human Stem Cells: From Degradation to Biosynthesis of Magnetic Nanoparticles Anew. *ACS Nano* **2020**, *14*, 1406−1417.
(39) Attaluri, A.; Ma, R.; Qiu, Y.; Li, W.; Zhu, L. Nanoparticle Distribution and Temperature Elevations in Prostatic Tumours in Mice during Magnetic Nanoparticle Hyperthermia. *Int. J. Hyperther.* **2011**, *27*, 491−502.
(40) Giustini, A. J.; Ivkov, R.; Hoopes, P. J. Magnetic Nanoparticle Biodistribution Following Intratumoral Administration. *Nanotechnology* **2011**, *22*, 345101.
(41) Kettering, M.; Richter, H.; Wiekhorst, F.; Bremer-Streck, S.; Trahms, L.; Kaiser, W. A.; Hilger, I. Minimal-invasive magnetic heating of tumors does not alter intra-tumoral nanoparticle accumulation, allowing for repeated therapy sessions: anin vivostudy in mice. *Nanotechnology* **2011**, *22*, 505102.
(42) Del Sol-Fernández, S.; Portilla-Tundidor, Y.; Gutiérrez, L.; Odio, O. F.; Reguera, E.; Barber, D. F.; Morales, M. P. Flower-like Mn-Doped Magnetic Nanoparticles Functionalized with $\alpha v\beta 3$-Integrin-Ligand to Efficiently Induce Intracellular Heat after Alternating Magnetic Field Exposition, Triggering Glioma Cell Death. *ACS Appl. Mater. Interfaces* **2019**, *11*, 26648−26663.
(43) Mazuel, F.; Espinosa, A.; Luciani, N.; Reffay, M.; Le Borgne, R.; Motte, L.; Desboeufs, K.; Michel, A.; Pellegrino, T.; Lalatonne, Y.; Wilhelm, C. Massive Intracellular Biodegradation of Iron Oxide Nanoparticles Evidenced Magnetically at Single-Endosome and Tissue Levels. *ACS Nano* **2016**, *10*, 7627−7638.
(44) Mejías, R.; Gutiérrez, L.; Salas, G.; Pérez-Yagüe, S.; Zotes, T. M.; Lázaro, F. J.; Morales, M. P.; Barber, D. F. Long Term Biotransformation and Toxicity of Dimercaptosuccinic Acid-Coated Magnetic Nanoparticles Support Their Use in Biomedical Applications. *J. Control. Release* **2013**, *171*, 225−233.
(45) Stepien, G.; Moros, M.; Pérez-Hernández, M.; Monge, M.; Gutiérrez, L.; Fratila, R. M.; de las Heras, M.; Menao Guillén, S.; Puente Lanzarote, J. J.; Solans, C.; Pardo, J.; de la Fuente, J. M. Effect of Surface Chemistry and Associated Protein Corona on the Long-Term Biodegradation of Iron Oxide Nanoparticles In Vivo. *ACS Appl. Mater. Interfaces* **2018**, *10*, 4548−4560.
(46) Lartigue, L.; Alloyeau, D.; Kolosnjaj-Tabi, J.; Javed, Y.; Guardia, P.; Riedinger, A.; Péchoux, C.; Pellegrino, T.; Wilhelm, C.; Gazeau, F. Biodegradation of Iron Oxide Nanocubes: High-Resolution in Situ Monitoring. *ACS Nano* **2013**, *7*, 3939−3952.
(47) Guzy, J.; Chakravarty, S.; Buchanan, F. J.; Chen, H.; Gaudet, J. M.; Hix, J. M. L.; Mallett, C. L.; Shapiro, E. M. Complex Relationship between Iron Oxide Nanoparticle Degradation and the Signal Intensity in Magnetic Particle Imaging. *ACS Appl. Nano Mater.* **2020**, *3*, 3991−3999.
(48) Fratila, R. M.; Navascuez, M.; Idiago-López, J.; Eceiza, M.; Miranda, J. I.; Aizpurua, J. M.; de la Fuente, M.; De La Fuente, J. M. Covalent immobilisation of magnetic nanoparticles on surfaces via

https://doi.org/10.1021/acsanm.2c03220
ACS Appl. Nano Mater. 2022, 5, 16220−16230

strain-promoted azide-alkyne click chemistry. *New J. Chem.* **2017**, *41*, 10835−10840.
(49) Mejías, R.; Pérez-Yagüe, S.; Gutiérrez, L.; Cabrera, L. I.; Spada, R.; Acedo, P.; Serna, C. J.; Lázaro, F. J.; Villanueva, M. A.; Morales, M. P.; Barber, D. F. Dimercaptosuccinic Acid-Coated Magnetite Nanoparticles for Magnetically Guided in Vivo Delivery of Interferon Gamma for Cancer Immunotherapy. *Biomaterials* **2011**, *32*, 2938−2952.

https://doi.org/10.1021/acsanm.2c03220
ACS Appl. Nano Mater. 2022, 5, 16220−16230